

The Ensemble Schrödinger Bridge filter for Nonlinear Data Assimilation

Hui Sun ^{*}

Abstract

This work puts forward a novel nonlinear optimal filter namely the Ensemble Schrödinger Bridge nonlinear filter. The proposed filter finds marriage of the standard prediction procedure and the diffusion generative modeling for the analysis procedure to realize one filtering step. The designed approach finds no structural model error, and it is derivative free, training free and highly parallelizable. Experimental results show that the designed algorithm performs well given highly nonlinear dynamics and nonlinear observation process in (mildly) high dimension up to 40 or above under a chaotic environment. It also shows better performance than classical methods such as the ensemble Kalman filter and the Particle filter in numerous tests given different level of nonlinearity. Future work will focus on extending the proposed approach to practical meteorological applications and establishing a rigorous convergence analysis.

keywords: Diffusion generative models, optimal filtering, training-free/derivative free generative models, Schrödinger Bridge, stochastic optimal control, data assimilation.

1 Introduction

Optimal filtering represents an important aspect for data assimilation task as it finds wide applications in weather forecasting, material sciences, biology, and finance [2, 3, 7, 8]. Optimal filtering is the process of estimating the hidden true states based on observed noisy states.

In science/engineering communities, the problem is usually casted under the Prediction-Analysis two step Bayesian framework where the goal is to accurately obtain/approximate the prior and posterior filtering densities. While the target densities are sometimes approximated by using the parametric method e.g. the plain vanilla Kalman Filter, they are more commonly tracked by using the *ensemble methods*.

The workhorse of the ensemble methods are the underlying simulation approaches. Two classical and state-of-the-art approaches under such framework are the *Ensemble Kalman Filter* (EnKF) and the *Particle Filter* (PF). Compared to the original Kalman filter, to more accurately approximate the filtering densities, EnKF utilizes an ensemble of particles for the estimate of statistical property of the system in the form of Gaussian distributions. As such, the target distribution is computed based on approximation from Gaussian densities. Such approach demonstrates limitations since it's very likely that the target density may be non-Gaussian with multi-modals. Hence, it is applicable effectively only for linear dynamics but cannot track accurately the highly non-linear ones. The PF approach, also known as the Sequential Monte Carlo method does not rely on any Gaussian/distributional assumption; instead, it relies on an ensemble of particles to approximate the filtering densities. This way, all information regarding the filtering densities is stored in the particle ensemble. Hence, the quality of the particle ensembles will determine the accuracy of density approximation, i.e. whether the particles are near the mode of the target density or if they can overall capture the configuration of the target density. It is observed that though PF demonstrates good performance in presence of nonlinearity, the performance deteriorates as dimension increases due to curse of dimensionality. In the high dimension regime, a tremendous

^{*}Department of Financial and Actuarial Mathematics, School of Mathematics and Physics, Xi'an Jiaotong-Liverpool University, Suzhou 215123, China. Email: Hui.Sun@xjtlu.edu.cn.

amount of particles are needed for a satisfactory approximation of the distribution which significantly limits the applicability of this approach.

Recently, by leveraging the idea from the generative diffusion models ([10, 13, 15, 18, 25]) a new Ensemble/simulation approach namely the Ensemble Score Filter (EnSF) is designed and proved to be very effective [1, 4, 5, 6]. Unlike the particle filters, the designed filter stores information in a *score function* and the update of approximated distribution at both the prediction and analysis steps amounts to updating the corresponding score function. The generation of particles then are based on a diffusion process (SDE) which leverages the score function as one component in the drift. Though shown to be very effective and efficient in high dimensions, this approach finds structural/model error in the simulation process as reported in [6]: an approximation is used in finding the posterior score. And so it results in bias in tracking the filtering densities with such limitation being more pronounced in lower dimensions given noisy observations (Example 4, Section 3.2.4.).

In this work, still following the Ensemble method/Simulation framework, we design a new diffusion process assisted nonlinear filter named the “Ensemble Schrödinger Bridge” filter (EnSBF) which implements analysis steps (particle generation) based on another type of diffusion SDE which we name the Schrödinger Bridge SDE (SB SDE). This SDE is induced by the solution to the “Schrödinger Bridge” problem [33], [34] [24]. And based on the solution to the SBP some numerical/deep learning algorithms are designed, [17, 18, 19, 21, 22, 24, 25] [9] and [26]. Of particular interests are those in [9] and [26] where generative tasks can be carried out without explicitly training neural networks. In this work, we further extended this approach to the dynamic/filtering setting and obtain a nonlinear data filter which is training free. Also, in contrast to the EnSF it is derivative free: during the entire updating procedure, no automatic differentiation with respect to either the exact state or the observational state is required. This approach also finds no model error: the only errors introduced at the particle generation step comes from the Euler approximation of the solution of SDE and the Monte Carlo (ensemble) approximation of integrals. Various numerical tests demonstrate that the EnSBF demonstrates competitive performs over both the classical PF and EnKF, and it provides a more reliable characterization of the distribution than the EnSF in the low dimension regime. In the meantime, we draw theoretically the direct connection between the SDE related to the solution of the SBP and the reverse SDE in the score-based diffusion model. Then, based on this connection we argue that one shall switch between the EnSBF and EnSF approach for filtering problems in the low and high dimension regime.

The paper is structured as follows: in Section 2 we give a brief discussion about the Schrödinger Bridge (SB) problem and its analytic solution. We first discuss the original formulation of SBP, discuss its control formulation and show the numerical algorithm which is the workhorse of the EnSBF we will design. We then discuss a general version of the SBP, discuss its solution and the control formulation. We show the direct connection between the reverse SDE in the score-based diffusion model and the SDE related to SBP under the control formulation. This helps us draw the connection between the designed EnSBF and EnSF. In Section 3, we review the optimal filtering problem and discuss the main algorithm for this paper. We then provide numerical examples where different level of nonlinearities and dimensions are considered, we remark that due to the direct connection between the SBP and the reverse process of the score-based diffusion models, we will switch to EnSF for higher dimensional applications. We then finish the paper with discussions on conclusion and future work.

2 The the Schrödinger bridge problem and the static algorithm

In this section, we introduce the Schrödinger bridge problem, present its solutions and explain the algorithm designed based on the same. Since the accuracy of the nonlinear filter relies on the reliability of the underlying simulation procedure, such procedure should not rely on any distributional assumption (unlike EnKF) and it should not introduce any structural error (unlike EnSF). The algorithm (static) designed based on the solution to SBP turned out to be a simple one-step simulation procedure which introduces no model structural error, hence it is used as the workhorse for the later (dynamic) nonlinear filter design (EnSBF). We comment that such static algorithm is a simple transformed version of the Schrödinger-Föllmer sampler, and was already studied in [9] and [26]. We defer the description of the (dynamic) EnSBF to the next section. We present two simulation

results based on this static algorithm and show that it can generate data samples which are statistically close to that of the given data sample given complex data structure. We comment that only Euler discretization and approximation via ensemble averaging are employed in the algorithm design and no further structural error is introduced. We then finish this section with showing the connection between the SB SDE and the reverse SDE in the score-based diffusion models which indicates that the current EnSBF is closely related to the EnSF.

2.1 The Schrödinger Bridge Problem (Original version)

The goal of the Schrödinger Bridge (SB) problem is to find a probability law on a path space so that it has the prescribed marginal distributions at the starting time and terminal time and that this probability law is required to minimize the loss with respect to the reference measure in terms of the relative entropy. More specifically, let $\Omega = C([0, 1]; \mathbb{R}^d)$ be the space of continuous functions on $[0, 1]$ valued in \mathbb{R}^d . Let $X = \{X_t\}_{t \in [0, 1]}$ be a canonical process on Ω where $X_t(\omega) = \omega_t, \omega \in \Omega$. The σ -field defined on Ω is the canonical σ -field $\mathcal{F} = \{\omega : (\omega_t)_{t \in [0, 1]} \in B \mid B \in \mathcal{B}(\mathbb{R}^d)\}$. Let $\mathcal{P}(\Omega)$ denote the space of probability measures on the path space Ω . Denoting $\mathbb{W}_{\sigma^2}^x$ as the law of BM starting from x with variance σ^2 , the law of reversible Brownian motion is defined via $\mathbb{Q}_{\sigma^2} = \int \mathbb{W}_{\sigma^2}^x dx$ so that its marginal is the Lebesgue measure at each time t . Note that \mathbb{Q}_{σ^2} is an unbounded measure on Ω . The original version of the Schrödinger's problem is formulated as follows:

Problem 1. (Schrödinger Bridge Problem.)

Find $\mathbb{P}^* \in \mathcal{P}(\Omega)$ such that

$$\mathbb{P}^* \in \arg \min_{\mathbb{P} \in \mathcal{P}(\Omega)} KL(\mathbb{P} \parallel \mathbb{Q}_{\sigma^2}) \quad (2.1)$$

with $\mathbb{P}_0^* = \nu$, $\mathbb{P}_1^* = \mu$ where the marginals are defined via the push forward: $\mathbb{P}_t(B) = (X_t \# \mathbb{P})(B) := \mathbb{P} \circ X_t^{-1}(B), B \in \mathcal{B}(\mathbb{R}^d), t \in [0, 1]$ and

$$\mathcal{H}(\mathbb{P} \parallel \mathbb{Q}) = \begin{cases} \int \ln \frac{d\mathbb{P}}{d\mathbb{Q}_{\sigma^2}} d\mathbb{P}, & \text{if } \mathbb{P} \ll \mathbb{Q}_{\sigma^2} \\ \infty, & \text{Otherwise} \end{cases} \quad (2.2)$$

The following theorem from [33] Theorem 2.8 provides characterizations of the solution to the SB problem.

Theorem 2.1. Let $\nu, \mu \ll \mathcal{L}_m$, then the SB problem admits a unique solution $\mathbb{P}^* = \int f^*(x)g^*(y)d\mathbb{Q}_{\sigma^2}^{xy}dxdy$ where f^*, g^* are \mathcal{L}_m -measurable nonnegative functions on \mathbb{R}^d satisfying the Schrödinger system of equations:

$$\begin{cases} f^*(x)\mathbb{E}_{\mathbb{Q}}[g^*(X_1)|X_0 = x] = \frac{d\nu}{d\mathcal{L}_m}(x), & \mathcal{L}_m - a.e. \\ g^*(y)\mathbb{E}_{\mathbb{Q}}[f^*(X_0)|X_1 = y] = \frac{d\mu}{d\mathcal{L}_m}(y), & \mathcal{L}_m - a.e.. \end{cases} \quad (2.3)$$

If we denote $f_0(x) := f^*(x)$ and $g_1(y) := g^*(y)$, and that $q(x) = \frac{d\nu}{d\mathcal{L}_m}(x)$, $p(x) = \frac{d\mu}{d\mathcal{L}_m}(x)$ the density of ν and μ , the transition density $h_{\sigma^2}(s, x, t, y) := (2\pi\sigma^2(t-s))^{-\frac{d}{2}} \exp(-\frac{|x-y|^2}{2\sigma^2(t-s)})$, then we have:

$$f_0(x) \int h_{\sigma^2}(0, x, 1, y)g_1(y)dy = q(x) \quad (2.4)$$

$$g_1(y) \int h_{\sigma^2}(0, x, 1, y)f_0(x)dx = p(y). \quad (2.5)$$

Further denoting $\int h_{\sigma^2}(0, x, 1, y)g_1(y)dy = g_0(x)$ and $\int h_{\sigma^2}(0, x, 1, y)f_0(x)dx = f_1(y)$, we have that the Schrödinger system can be characterized by:

$$\begin{aligned} q(x) &= f_0(x)g_0(x) \\ p(y) &= f_1(x)g_1(y) \end{aligned} \quad (2.6)$$

with the following forward and backward equations on $(0, 1) \times \mathbb{R}^d$ [34]:

$$\begin{cases} \partial_t f_t(x) = \frac{\sigma^2}{2} \Delta f_t(x), \\ \partial_t g_t(x) = -\frac{\sigma^2}{2} \Delta g_t(x). \end{cases}$$

Following again [34], let q_t denote the density of \mathbb{P}_t^* , then this density function is given via:

$$q_t(x) = f_t(x)g_t(x). \quad (2.7)$$

Theorem 3.1 and 3.2 in [24] shows that the SB problem also has a control formulation whose solution (optimal control) is given by $\alpha_t^*(x) = \sigma^2 \nabla_x \log \int h_{\sigma^2}(t, x, 1, y)g_1(y)dy$:

Problem 2. (Control Formulation)

$$\alpha_t^*(x) \in \arg \min_{\alpha \in \mathcal{U}} \frac{1}{2} \mathbb{E} \left[\int_0^1 \|\alpha_t\|^2 dt \right] \quad (2.8)$$

under the constraint: $\mathcal{L}(X_T) = \mu$ where

$$dX_t = \alpha_t dt + \sigma dW_t, \quad X_0 \sim \nu. \quad (2.9)$$

\mathcal{U} is collection of all adapted process such that

$$\mathbb{E} \left[\int_0^T |\alpha_s|^2 ds \right] < \infty. \quad (2.10)$$

Note that Problem 2 is particularly useful since it provides a systematic way for simulation once the optimal control α_t is available. That is, let $\mu := p_{data}$ be the target distribution, then one obtains the particle ensemble approximation to μ by transporting a particle cloud starting approximating $q(x)$ via (2.9) and obtain an ensemble at time $T = 1$.

Based on the discussion above, we discuss an example with designed initial and target distribution. Denoting $\phi_\sigma(x) := \frac{1}{(2\pi\sigma^2)^{\frac{d}{2}}} \exp(-\frac{|x|^2}{2\sigma^2})$ the density function of a Gaussian distribution, then:

Assuming $p_{data} \ll \mathcal{L}_m$, and we set $\mu := p_{data}$. Take $f^*(x) = f_0(x) = \delta_0(x)$, $g_1(y) = \frac{p(y)}{\phi_\sigma(y)}$ we can check that:

$$g_1(y) \int h_{\sigma^2}(0, x, 1, y) f_0(x) dx = p(y) \quad (2.11)$$

$$f_0(x) \int h_{\sigma^2}(0, x, 1, y) g_1(y) dy = q(x) \quad (2.12)$$

since the first equation gives $g_1(y) = \frac{p(y)}{\phi_\sigma(y)}$ and the second equation holds due to the equality $\int h_{\sigma^2}(0, 0, 1, y) g_1(y) dy = 1$. Now, set $\sigma = 1$ and by the solution of Problem 2 we have,

$$\alpha_t(x) = \nabla_x \log \mathbb{E}_{Z \sim \mu_W} \left[\frac{\mu}{\mu_W} (x + \sqrt{T-t}Z) \right]. \quad (2.13)$$

Thus, to sample from the target distribution μ , one just need to start with δ_0 and follow the stochastic dynamics:

$$dX_t = \alpha_t(X_t) dt + \sigma dW_t, \quad X_0 \sim \delta_0(x), \quad T = 1. \quad (2.14)$$

This is the famous Schrödinger-Föllmer sampler. We will discuss another similar design based on (2.4) in Example 2.1.

2.1.1 Algorithm based on the solution to the SB problem.

In this work, we focus on (2.13) for algorithm design due to its simplicity and effectiveness (shown later) and point out the fact that the appropriate level of noise (σ) added still needs to be explored.

After a change of measure, equation (2.13) can be equivalently written as ($T = 1$):

$$\begin{aligned} \alpha_t(x) &= \nabla_x \log \mathbb{E}_{Z \sim \mu_W} \left[\frac{\mu}{\mu_W} (x + \sqrt{T-t}Z) \right] \\ &= \nabla_x \log \mathbb{E}_{Z \sim \mu} \left[\exp \left(-\frac{1}{2(T-t)} |Z - x|^2 + \frac{1}{2T} |Z|^2 \right) \right] \end{aligned} \quad (2.15)$$

$$\begin{aligned} &= \frac{\mathbb{E}_{Z \sim \mu} [(Z - x) \exp \left(-\frac{1}{2(T-t)} |Z - x|^2 + \frac{1}{2T} |Z|^2 \right)]}{(T-t) \mathbb{E}_{Z \sim \mu} [\exp \left(-\frac{1}{2(T-t)} |Z - x|^2 + \frac{1}{2T} |Z|^2 \right)]}. \end{aligned} \quad (2.16)$$

Now the solution shown in the form of (2.16) contains expectation taken under the data measure. In simulation, such form will be useful when one only has access to samples following the data distribution. Equivalently though, equation (2.13) finds expectation taken under the standard Gaussian measure. This form will become useful when the target measure μ is absolutely continuous with respect to the Lebesgue measure and when the analytic formula for μ is known. See [35] for more detailed discussion.

We note that to perform data generation following the target distribution μ , one needs to discretize the diffusion process (2.14) and approximate expectation in (2.16) with Monte Carlo method, that is

$$\alpha(t, x) \approx \frac{\sum_{i=1}^M (Z^i - x) \exp(-\frac{1}{2(T-t)}|Z^i - x|^2 + \frac{1}{2T}|Z^i|^2)}{(T-t) \sum_{i=1}^M \exp(-\frac{1}{2(T-t)}|Z^i - x|^2 + \frac{1}{2T}|Z^i|^2)} := \alpha^M(t, x). \quad (2.17)$$

where M denotes the size of the data ensemble. And the solution of the SDE can be approximated by the following:

$$X_{t_{n+1}}^{M,N} = X_{t_n}^{M,N} + \alpha^M(t_n, X_{t_n}^{M,N}) \Delta t + \Delta W_{t_n}, \quad X_{t_0}^{M,N} = 0. \quad (2.18)$$

As such, we use the following algorithm for the generation of the artificial data from target distribution μ . The algorithm for the Schrödinger Bridge data generator is summarized in Algorithm 1, and α^M is defined as in (2.17). We note that similar algorithm can be found in the literature [9, 26]. We provide two numerical examples

Algorithm 1 Algorithm for producing generative samples based on Schrödinger Bridge solution.

Require: Initializing the following

- The data collection $\{Z_i\}_{i=1,\dots,M}$ which forms an empirical measure $\frac{1}{M} \sum_{i=1}^M \delta_{Z_i}$.
- The initial ensemble collection $\{X_{t_0}^{M,N,\iota}\}_{\iota=1,\dots,B}$ which all start from 0.
- Total number of temporal discretization N , with terminal time $T = 1$.

- 1: **for** $n = 0, 1, \dots, N - 1, \iota \in \{1, 2, \dots, B\}$ **do**
- 2: For each particle, update its position based on the following dynamics:

$$X_{t_{n+1}}^{M,N,\iota} = X_{t_n}^{M,N,\iota} + \alpha^M(t_n, X_{t_n}^{M,N,\iota}) \Delta t + \Delta W_{t_n}, \quad X_{t_0}^{M,N,\iota} = 0. \quad (2.19)$$

- 3: **end for**
- 4: **return** The collection of generated particles $\{X_1^{M,N,\iota}\}_{\iota=1,\dots,B}$.

in section 2.5 to demonstrate that such algorithm performs well on dataset with complex distribution in high dimensions.

Note that the SDE (2.14) induces an ‘identity’ map $A : \mathcal{P}(\Omega) \rightarrow \mathcal{P}(\Omega)$ which maps the given data distribution μ to itself. In a similar fashion, the numerical scheme (2.19) induces a map $A^B : \mathcal{P}(\Omega) \rightarrow \mathcal{P}(\Omega)$ via:

$$A^B \mu = \frac{1}{B} \sum_{\iota=1}^B \delta_{X_1^{M,N,\iota}} \quad (2.20)$$

where $X_1^{M,N,\iota}$ is the terminal state of solution of (2.19) and B denotes the total number of simulated final states collected. To summarize, this operator takes the target μ , perform particle approximation and then generate data points with the discretized SDE. Then the target distribution is approximated by particle ensemble of the terminal state.

To see that the Schrödinger Bridge data generator can produce new data which is statistically close to the original dataset, we implement the discretized SDE (2.19) in Algorithm 1. The distribution of the terminal state X_T is finally approximated by particle ensemble accordingly.

As a first example, we make use of the Moons dataset and manage to generate new artificial data which follows approximately the same distribution. The dataset is available from the Sklearn built-in data library

named ‘make moons’ where total 1000 data points are available. Those data points are plotted as orange dots in figure 1a. The artificial dataset obtained is shown as blue dots accordingly. The approximated ensemble is of size 400 and it was generated under the discretized diffusion process with total time steps $N = 1024$. This preliminary example shows the soundness of the proposed Schrödinger Bridge data generator.

As a second example, we use the standard handwritten digits dataset for data generation purpose. The dataset contains 10000 data samples of various digits and each sample is an image of pixel size $1 \times 28 \times 28$. Thus, this example is used to demonstrate that the algorithm performs also in higher dimensions. In our experiment, we generate artificial digits by using only 100 samples to test the algorithm performance. The result in 1b shows that Algorithm 1 produce good results even given small input data samples.

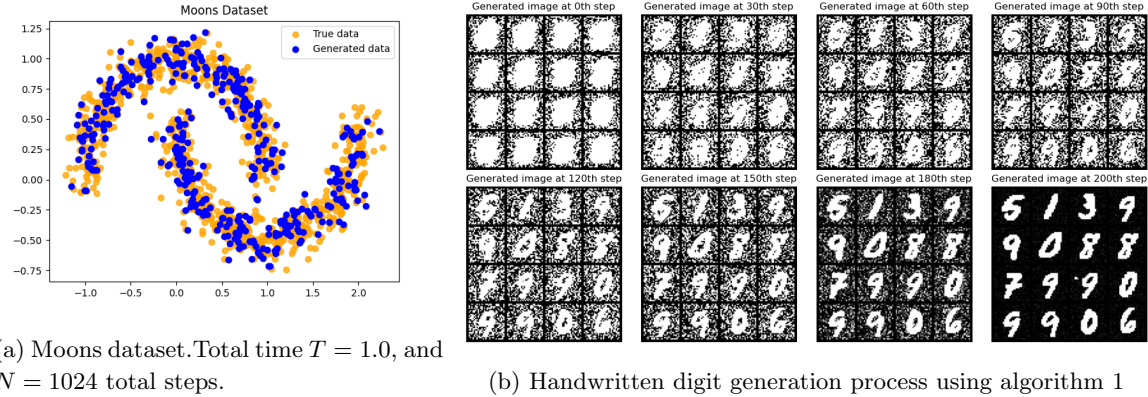


Figure 1: Demonstration for Algorithm 1. Two numerical examples are presented to show that the algorithm can capture the complicated structure of the underlying distribution (data) by producing samples which are statistically close to the original ones.

2.2 Schrödinger bridge problem with general reference measure

For a more generalized Schrödinger bridge problem, we consider the following:

Problem 3. (Schrödinger Bridge Problem with general coefficients.) Let \mathbb{Q}^x be the reference measure induced by the following SDE:

$$dX_t = b_t X_t dt + \sigma_t dW_t, \quad X_0 = x \quad (2.21)$$

where b_t and σ_t are time deterministic function. Define $\mathbb{Q} := \int \mathbb{Q}^x q_0(x) dx$ where q_0 is a probability density function. Find $\mathbb{P}^* \in \mathcal{P}(\Omega)$ such that

$$\mathbb{P}^* \in \arg \min_{\mathbb{P} \in \mathcal{P}(\Omega)} KL(\mathbb{P} || \mathbb{Q}) \quad (2.22)$$

with $\mathbb{P}_0^* = \nu$, $\mathbb{P}_1^* = \mu$ and

$$\mathcal{H}(\mathbb{P} || \mathbb{Q}) = \begin{cases} \int \ln \frac{d\mathbb{P}}{d\mathbb{Q}} d\mathbb{P}, & \text{if } \mathbb{P} \ll \mathbb{Q} \\ \infty, & \text{Otherwise} \end{cases} \quad (2.23)$$

By the disintegration of measure ([33], A.8):

$$H(\mathbb{P} || \mathbb{Q}) = H(\mathbb{P}_{01} || \mathbb{Q}_{01}) + \int H(\mathbb{P}^{xy} || \mathbb{Q}^{xy}) \mathbb{P}_{01}(dxdy) \quad (2.24)$$

where $\mathbb{P}^{xy} = \mathbb{E}^{\mathbb{P}}[\cdot | X_0 = x, X_1 = y]$, $\mathbb{Q}^{xy} = \mathbb{E}^{\mathbb{Q}}[\cdot | X_0 = x, X_1 = y]$ are the conditional probabilities, and $\mathbb{P}_{01}, \mathbb{Q}_{01}$ are the joint distributions of (X_0, X_1) under the two measures. We see that by choosing $\mathbb{P}^{xy} = \mathbb{Q}^{xy}$, the original problem 3 is reduced to the following static Schrödinger Bridge problem.

Problem 4. Given $\mathbb{Q}_{01} \in \mathcal{M}_+(\mathbb{R}^d \times \mathbb{R}^d)$ where \mathbb{Q}_{01} is the joint distribution between (X_0, X_1) defined in Problem 3 between time zero and one. Find

$$\pi^* \in \arg \min_{\pi \in \mathcal{P}(\mathbb{R}^d \times \mathbb{R}^d)} KL(\pi || \mathbb{Q}_{01}), \quad \pi_0 = \nu, \quad \pi_1 = \mu. \quad (2.25)$$

where ν and μ are the prescribed measures.

The problem is solved by using the Lagrange multipliers, i.e. let:

$$\mathcal{L}(\pi, \lambda, \gamma) := \int \pi(x, y) \log \frac{\pi(x, y)}{\mathbb{Q}_{01}(x, y)} dx dy + \int \lambda(x) \left(\int \pi(x, y) dy - \rho_\nu(x) \right) dx + \int \gamma(y) \left(\int \pi(x, y) dx - \rho_\mu(y) \right) dy \quad (2.26)$$

Setting the first variation to 0 to obtain:

$$1 + \log \pi(x, y) - \log \mathbb{Q}_{01}(x, y) + \lambda(x) + \gamma(y) = 0. \quad (2.27)$$

Noting that $\mathbb{Q}_{01}(x, y) = q(0, x, 1, y)q_0(x)$ where $q(0, x, 1, y)$ is the transition density. After rearranging, we obtain

$$\pi(x, y) = f_0(x)q(0, x, 1, y)g_1(y) \quad (2.28)$$

for some function $f_0(x)$ and $g_1(y)$ which satisfy the following integral constraint:

$$f_0(x) \int q(0, x, 1, y)g_1(y) dy = \rho_\nu(x) \quad (2.29)$$

$$g_1(y) \int q(0, x, 1, y)f_0(x) dx = \rho_\mu(y). \quad (2.30)$$

Defining

$$\int q(0, x, 1, y)g_1(y) dy = g_0(x) \quad (2.31)$$

$$\int q(0, x, 1, y)f_0(x) dx = f_1(y). \quad (2.32)$$

we then obtain the following system of equations:

$$f_0(x)g_0(x) = \rho_\nu(x) \quad (2.33)$$

$$g_1(y)f_1(y) = \rho_\mu(y). \quad (2.34)$$

Thus, using (2.28) the measure defined by

$$\mathbb{P}^*(\cdot) = \int \mathbb{Q}^{xy}(\cdot) \pi(x, y) dx dy \quad (2.35)$$

solves the Schrödinger bridge problem 3.

By defining

$$\alpha(t, x) = \nabla \log \int q(t, x, 1, y)g_1(y) dy \quad (2.36)$$

then due to [24] Theorem 3.2, we have that $\alpha(t, x)$ solves the following optimal control problem

Theorem 2.2. ([24] *Theorem 3.1*)

$$\alpha_t^*(x) \in \arg \min_{\alpha \in \mathcal{U}} \frac{1}{2} \mathbb{E} \left[\int_0^1 \|\alpha_t\|^2 dt \right] \quad (2.37)$$

under the constraint: $\mathcal{L}(X_T) = \mu$ where

$$dX_t = (b_t X_t + \alpha_t) dt + \sigma_t dW_t, \quad X_0 \sim \rho_\nu(x). \quad (2.38)$$

\mathcal{U} is collection of all adapted process such that

$$\mathbb{E} \left[\int_0^T |\alpha_s|^2 ds \right] < \infty. \quad (2.39)$$

2.3 Connecting the Schrödinger Bridge problem with Score-based diffusion models

Now we establish the connection between the solution of Schrödinger bridge problem with score-based diffusion models. Recall that for the score-based diffusion model [36], the forward and backward processes are as follows:

$$dX_t = \tilde{b}(t, X_t) dt + \tilde{\sigma}(t, X_t) dW_t, \quad X_0 \sim p_{data}, \quad X_T \sim p(T, x) \quad (2.40)$$

$$dY_t = (-\tilde{b}(T-t, Y_t) + \frac{\nabla \cdot (p(T-t, Y_t) \tilde{a}(T-t, Y_t))}{p(T-t, Y_t)}) dt + \tilde{a}_{T-t} dW_t, \quad Y_0 \sim p(T, x), \quad Y_T \sim p_{data}(x) \quad (2.41)$$

where $\tilde{a} := \tilde{\sigma} \tilde{\sigma}^T$.

For analytic trackability, we consider the following linear SDE (2.42) with the corresponding reverse SDE (2.43) with $T = 1$.

$$dX_t = \tilde{b}(t) X_t dt + \tilde{\sigma}(t) dW_t, \quad X_0 \sim p_{data}, \quad X_1 \sim p(1, x) \quad (2.42)$$

$$dY_t = \left(-\tilde{b}(1-t) Y_t dt + \tilde{a}_{1-t} \nabla \log p(1-t, Y_t) \right) dt + \tilde{\sigma}_{1-t} dW_t, \quad Y_0 \sim p(1, x), \quad Y_1 \sim p_{data}(x) \quad (2.43)$$

where both $\tilde{b}(t), \tilde{\sigma}(t)$ are time deterministic functions, $p(1, x) = \int \tilde{q}(0, y, 1, x) p_{data}(y) dy$. The solution of (2.42) given $X_{t_0} = x$ is the following:

$$X_t = e^{\int_{t_0}^t \tilde{b}_s ds} x + e^{\int_{t_0}^t \tilde{b}_s ds} \int_{t_0}^t e^{-\int_{t_0}^s \tilde{b}_r dr} \tilde{\sigma}_s dW_s \quad (2.44)$$

The transition density is given as

$$\tilde{q}(t_0, x, t, y) = \frac{1}{\sqrt{2\pi \tilde{\sigma}_{t_0, t}^2}} \exp \left(-\frac{(y - \tilde{\mu}_{t_0, t} x)^2}{2\tilde{\sigma}_{t_0, t}^2} \right) \quad (2.45)$$

where $\tilde{\mu}_{t_0, t} = e^{\int_{t_0}^t \tilde{b}_s ds} x$ and $\tilde{\sigma}_{t_0, t}^2 = e^{2 \int_{t_0}^t \tilde{b}_s ds} \int_{t_0}^t e^{-2 \int_{t_0}^s \tilde{b}_r dr} \tilde{\sigma}_s^2 ds = \int_{t_0}^t e^{2 \int_s^t \tilde{b}_r dr} \tilde{\sigma}_s^2 ds$.

Theorem 2.3. *The score function of solution to the SDE (2.42) with $X_0 \sim p_{data}(x)$ evaluated at time $1-t$ is given by the optimal control α^* to the stochastic optimal control problem 2.2 at time t ,*

$$dX_t = b_t X_t dt + \alpha(t, X_t) dt + \sigma_t dW_t, \quad X_0 \sim \rho_\nu, \quad X_T \sim \rho_\mu \quad (2.46)$$

with $\rho_\nu \sim \int q(0, x, 1, y) p_{data}(y) e^{I_{0,1}} dy$ and $\rho_\mu \sim p_{data}$, where $b_t := -\tilde{b}_{1-t}$, $\sigma_t := \tilde{\sigma}_{1-t}$ and $q(0, x, 1, y)$ is the transition density of the SDE:

$$dX_t = b_t X_t dt + \sigma_t dW_t, \quad X_0 = x. \quad (2.47)$$

Proof. Consider the score function of X_t which is the solution to (2.42),

$$\begin{aligned}
\nabla \log p(1-t, y) &= \nabla \log \int \tilde{q}(0, x, 1-t, y) p_{data}(x) dx \\
&= \nabla \log \frac{1}{\sqrt{2\pi\tilde{\sigma}_{0,1-t}^2}} \int \exp\left(-\frac{|y - \tilde{\mu}_{0,1-t}x|^2}{2\tilde{\sigma}_{0,1-t}^2}\right) p_{data}(x) dx \\
&= \nabla \log \frac{1}{\sqrt{2\pi\tilde{\sigma}_{0,1-t}^2}} \int \exp\left(-\frac{|\tilde{\mu}_{0,1-t}^{-1}y - x|^2}{2(\tilde{\sigma}_{0,1-t}/\tilde{\mu}_{0,1-t})^2}\right) p_{data}(x) dx
\end{aligned} \tag{2.48}$$

Note that by a change of variable:

$$\tilde{\mu}_{0,1-t}^{-1} = \exp\left(-\int_0^{1-t} \tilde{b}_s ds\right) = \exp\left(\int_t^1 -\tilde{b}_{1-r} dr\right)$$

$$\tilde{\sigma}_{0,1-t}^2 = \int_t^1 e^{2\int_s^t -\tilde{b}_{1-h} dh} \tilde{\sigma}_{1-s}^2 ds \tag{2.49}$$

$$\tilde{\sigma}_{0,1-t}^2 / \tilde{\mu}_{0,1-t}^2 = \int_t^1 e^{2\int_s^1 -\tilde{b}_{1-r} dr} \tilde{\sigma}_{1-s}^2 ds \tag{2.50}$$

by letting

$$b_t = -\tilde{b}_{1-t}, \quad \sigma_t = \tilde{\sigma}_{1-t} \tag{2.51}$$

we define a new SDE where we denote its transition kernel by $q(t, x, 1, y)$:

$$dX_s = b_s X_s ds + \sigma_s dW_s, \quad X_t = x \tag{2.52}$$

we have that:

$$\sigma_{t,1}^2 = \int_t^1 e^{2\int_s^1 b_r dr} \sigma_s^2 ds = \tilde{\sigma}_{0,1-t}^2 / \tilde{\mu}_{0,1-t}^2 \tag{2.53}$$

$$\mu_{t,1} = \exp\left(\int_t^1 b_r dr\right) = \tilde{\mu}_{0,1-t}^{-1} \tag{2.54}$$

As a result, we have the following sequence of equalities:

$$(2.48) = \nabla \log \int \frac{1}{\sqrt{2\pi\sigma_{t,1}^2 \mu_{t,1}^{-2}}} \exp\left(-\frac{|\mu_{t,1}y - x|^2}{2\sigma_{t,1}^2}\right) p_{data}(x) dx \tag{2.55}$$

$$= \nabla \log \int q(t, y, 1, x) p_{data}(x) \mu_{t,1} dx \tag{2.56}$$

$$= \nabla \log \int q(t, y, 1, x) p_{data}(x) dx \tag{2.57}$$

where the term $\mu_{t,1}$ is dropped due to gradient operator. Also the above argument leads to following identity

$$\int q(t, x, 1, y) p_{data}(y) \mu_{t,1} dy = \int \tilde{q}(t, y, 1, x) p_{data}(y) dy. \tag{2.58}$$

Next, note that the SBP with \mathbb{Q}^x induced by (2.52), and the initial density $\rho_\nu(x) = \int q(0, x, 1, y) p_{data}(y) e^{I_{0,1}} dy$ and the target density $p_{data}(y)$, (2.29) and (2.30) are satisfied with $f_0(x) = 1$ and $g_1(y) = p_{data}(y) e^{I_{0,1}}$, where $I_{t_0,t} := \int_{t_0}^t b_s ds$. Hence by Theorem 2.2, we have

$$\alpha^*(t, x) := a_{1-t} \nabla \log \int q(t, x, 1, y) p_{data}(y) e^{I_{0,1}} dy \tag{2.59}$$

$$= a_{1-t} \nabla \log \int q(t, x, 1, y) p_{data}(y) dy \tag{2.60}$$

solves the corresponding optimal control problem and in particular

$$dX_t = \left(b_t X_t + \alpha^*(t, X_t) \right) dt + \sigma_t dW_t, \quad X_0 \sim \nu, \quad X_T \sim \mu \quad (2.61)$$

with $\rho_\nu = \int q(0, x, 1, y) p_{data}(y) e^{f_0} dy$, $\rho_\mu(x) = p_{data}(x)$. And we see that (2.57) is exactly (2.60) with a change of dummy variable. \square

Example 2.1. We first consider an example in the original SBP setup, where we have $b_t = 0$ and $\sigma_t = \sigma$ a constant. We consider the case where data samples may present sparsity or spikes, hence a smoothed/regularized version of the data is learned first which is obtained by adding noise to the same. Then to learn the true density, one endeavors to carry out a denoising procedure. This is part of the motivation for [13]. As such, we first take the target measure to be $p_{\sigma, data} := \int p_{data}(y) \phi_\sigma(x - y) dy$ and will recover the target measure p_{data} from the same. Hence we formulate the following two step procedure:

$$dX_t = \sigma \nabla \log \mathbb{E}^{Z \sim \phi_\sigma} \left[\frac{p_{\sigma, data}}{\phi_\sigma} (X_t + \sqrt{1-t} Z) \right] dt + \sigma dW_t, \quad X_0 = 0 \quad (2.62)$$

$$dX_t = \sigma^2 \nabla p_{\sqrt{1-t}\sigma, data}(X_t) dt + \sigma dW_t, \quad X_0 \sim p_{\sigma, data} \quad (2.63)$$

Equation (2.62) can be obtained in a similar fashion as (2.11) by setting $\mu := p_{\sigma, data}$ in the first step. Equation (2.63) is then obtained by setting $f_0(x) = 1$ so that $g_1(y) = p_{data}(y)$. And one can check that $q(x) = \int p_{data}(y) h_\sigma(0, x, 1, y) dy = p_{\sigma, data}$ is the smoothed data distribution. Note that (2.63) has recovered the reverse denoising process from the score-based diffusion model.

Example 2.2. (Recovering the set up for score-based diffusion models) As a special case, in [1], the forward processes are taken to be

$$\tilde{b}_t = \frac{d \log \alpha_t}{dt} \quad (2.64)$$

$$\tilde{\sigma}_t^2 = \frac{d \beta_t^2}{dt} - 2 \frac{d \log \alpha_t}{dt} \beta_t^2, \quad \alpha_t = 1 - t, \quad \beta_t^2 = t. \quad (2.65)$$

where the benefit is that the initial data distribution will be transformed into pure noise (Gaussian distribution) at $T = 1$. We point out that there is singularity near the terminal time $T = 1$. The forward SDE takes the form:

$$dX_t = \tilde{b}_t X_t dt + \tilde{\sigma}_t dW_t, \quad \rho_{X_0} = p_{data} \quad (2.66)$$

As such, for the Schrödinger Bridge problem, the reference SDE is given by

$$dX_t = -\tilde{b}_{1-t} X_t dt + \tilde{\sigma}_{1-t} dW_t, \quad X_0 = x. \quad (2.67)$$

And the controlled SDE with $\alpha^*(t, x) = \tilde{a}_{1-t} \nabla \log \int q(t, x, 1, y) g_1(y) dy$ takes the form:

$$dX_t = \left(-\tilde{b}_{1-t} X_t + \tilde{a}_{1-t} \nabla \log \int q(t, X_t, 1, y) g_1(y) dy \right) dt + \tilde{\sigma}_{1-t} dW_t$$

with $X_0 \sim \int q(0, x, 1, y) p_{data}(y) e^{f_0} dy = \int \tilde{q}(0, y, 1, x) p_{data}(y) dy = \Phi(x)$, $X_T \sim p_{data}(x)$, where $\Phi(x)$ is standard Gaussian. Note that this is the backward process for (2.66):

$$dX_t = \left(-\tilde{b}_{1-t} X_t + \tilde{a}_{1-t} \nabla \log \tilde{p}(1-t, X_t) \right) dt + \tilde{\sigma}_{1-t} dW_t \quad (2.68)$$

with $X_0 \sim \int \tilde{q}(0, x, 1, y) p_{data}(y) dy = \Phi(x)$, $X_T \sim p_{data}(x)$.

As a result, according to the discussion above, the backward process of the diffusion model is precisely given by the SDE related to the solution of the Schrödinger bridge problem under the stochastic optimal control (SOC) formulation. And the SBP formulation can in fact provide larger varieties of the distribution generation procedures, see for instance equation (2.13) and Example 2.1. Hence, we further comment that the score-based diffusion model can be treated as a special case of the controlled SDE related to the Schrödinger bridge problem which gives us mathematical reasons for switching between the EnSBF and EnSF methods under different dimension regimes.

3 Filtering problem, discrete setting

In this section, we design a nonlinear filter which we name the Ensemble Schrödinger Bridge filter based on the training free Schrödinger bridge data generator introduced earlier. Before presentation of the new algorithm, we briefly review the filtering problem and the classical particle method which is used as our main benchmark.

We consider a stochastic dynamical system of the following form:

$$X_{j+1} = f(X_j, \omega_j), \quad \text{Exact signal} \quad (3.1)$$

$$Y_{j+1} = g(X_{j+1}) + \epsilon_{j+1}, \quad \text{Observation} \quad (3.2)$$

where $X \in \mathbb{R}^d$, $Y \in \mathbb{R}^n$, $\epsilon \in \mathbb{R}^n$, $\omega \in \mathbb{R}^m$ and the noise terms ω, ϵ are taken to be Gaussian random variables which are independent. The goal of the filtering problem is to estimate X_{j+1} given the observations $\mathcal{Y}_{j+1} := \{Y_l\}_{l=0}^{j+1}$ where the later corresponds to observations of one path. Mathematically, one endeavors to find the filtering density

$$\mathbb{P}(X_{j+1} | \mathcal{Y}_{j+1}), \quad \forall j \in \{0, 1, \dots, J-1\} \quad (3.3)$$

where J denotes the total filtering steps. One well-established approach for solving the same is via the Bayesian filter framework; namely one sequentially iterates the following two steps:

- **Prediction step.** Given the posterior $\mathbb{P}(X_j | \mathcal{Y}_j)$ at step j and the transition probability $\mathbb{P}(X_{j+1} | X_j)$, one finds the prior filtering density as follows:

$$\mathbb{P}(X_{j+1} | \mathcal{Y}_j) = \int \mathbb{P}(X_{j+1} | X_j) \mathbb{P}(X_j | \mathcal{Y}_j) dX_j. \quad (3.4)$$

This step is based on the Chapman-Kolmogorov formula, and we denote by $\tilde{\mu}_{j+1} = \mathbb{P}(X_{j+1} | Y_j)$.

- **Update step.** To obtain posterior density at step $j+1$, one combines the likelihood function $\mathbb{P}(Y_{j+1} | X_{j+1})$ with the prior

$$\mathbb{P}(X_{j+1} | \mathcal{Y}_{j+1}) \propto \mathbb{P}(Y_{j+1} | X_{j+1}) \mathbb{P}(X_{j+1} | \mathcal{Y}_j) \quad (3.5)$$

This step is based on the Bayesian inference [32], where

$$\mathbb{P}(Y_{j+1} | X_{j+1}) \sim \exp \left(-\frac{1}{2} (g(X_{j+1}) - Y_{j+1})^T \Sigma^{-1} (g(X_{j+1}) - Y_{j+1}) \right) \quad (3.6)$$

and $\Sigma = \text{Cov}(\epsilon)$ is the covariance matrix of the noise in (3.2).

We note that this step corresponds to a map: $G_j : \mathcal{P}(\Omega) \rightarrow \mathcal{P}(\Omega)$ such that

$$G_j \tilde{\mu}_{j+1} = \frac{\tilde{g}_j \tilde{\mu}_{j+1}(dx)}{\int_{\mathbb{R}^d} \tilde{g}_j(x) \tilde{\mu}_{j+1}(dx)} := \mu_{j+1} \quad (3.7)$$

where $\mu_{j+1} = \mathbb{P}(X_{j+1} | \mathcal{Y}_{j+1})$, and $\tilde{g}_j(X_{j+1}) \sim \mathbb{P}(Y_{j+1} | X_{j+1})$.

3.1 Design of the Schrödinger Bridge nonlinear filter

To design the Schrödinger Bridge nonlinear filter, similar to the particle filter approach for the prediction step, we update the particle location based on dynamics (3.1) to obtain $\{\tilde{X}_{j+1}\}$ and approximate $\mathbb{P}(X_{j+1} | \mathcal{Y}_j)$ via $\frac{1}{B} \sum_{i=1}^B \delta_{\tilde{X}_{j+1}^i}$.

For the analysis step, the target distribution is μ_{j+1} as in (3.7), and we endeavor to generate samples from this distribution via the Schrödinger Bridge data generator (Algorithm 1).

To highlight the fact that the target distribution is μ_{j+1} at the j th filtering step, we write $\alpha(t, x, \mu_{j+1})$ to denote such dependence. Note that the drift term can be written as follows:

$$\begin{aligned}\alpha(t, x, \mu_{j+1}) &= \frac{\int (z - x) \exp(-\frac{1}{2(T-t)}|z - x|^2 + \frac{1}{2T}|z|^2) d\mu_{j+1}(z)}{(T-t) \int \exp(-\frac{1}{2(T-t)}|z - x|^2 + \frac{1}{2T}|z|^2) d\mu_{j+1}(z)} \\ &= \frac{\int (z - x) \exp(-\frac{1}{2(T-t)}|z - x|^2 + \frac{1}{2T}|z|^2) \tilde{g}_j(z) d\tilde{\mu}_{j+1}(z)}{(T-t) \int \exp(-\frac{1}{2(T-t)}|z - x|^2 + \frac{1}{2T}|z|^2) \tilde{g}_j(z) d\tilde{\mu}_{j+1}(z)} \\ &= \frac{\mathbb{E}_{Z \sim \tilde{\mu}_{j+1}}[(Z - x) \exp(-\frac{1}{2(T-t)}|Z - x|^2 + \frac{1}{2T}|Z|^2) \tilde{g}_j(Z)]}{(T-t) \mathbb{E}_{Z \sim \tilde{\mu}_{j+1}}[\exp(-\frac{1}{2(T-t)}|Z - x|^2 + \frac{1}{2T}|Z|^2) \tilde{g}_j(Z)]} =: \tilde{\alpha}(t, x, \tilde{\mu}_{j+1}),\end{aligned}\quad (3.8)$$

where in the second equality above, the normalizing constant $\int_{\mathbb{R}^d} \tilde{g}_j(z) \tilde{\mu}_j(dz)$ was canceled. Using $\tilde{\alpha}$ as the drift, one obtains a map $\tilde{A}_j : \mathcal{P}(\Omega) \rightarrow \mathcal{P}(\Omega)$ such that $\tilde{A}_j \tilde{\mu}_{j+1} = \mu_{j+1}$.

Since $\tilde{\mu}_{j+1}$ is not known analytically, i.i.d samples from the same are used for numerical integration in (3.8). That is, one adopts the following approximation for numerical implementation:

$$\tilde{\alpha}(t, x, \tilde{\mu}_{j+1}) \approx \frac{\sum_{i=1}^B (Z^i - x) \tilde{g}_j(Z^i) \exp(-\frac{1}{2(T-t)}|Z^i - x|^2 + \frac{1}{2T}|Z^i|^2)}{(T-t) \sum_{i=1}^B \tilde{g}_j(Z^i) \exp(-\frac{1}{2(T-t)}|Z^i - x|^2 + \frac{1}{2T}|Z^i|^2)}.\quad (3.9)$$

where $Z^i \sim \tilde{\mu}_{j+1}$.

Based on the above discussion, we can approximate target distribution by its empirical distribution with M particles and define an approximation $\tilde{A}_j^{N,M} : \mathcal{P}(\Omega) \rightarrow \mathcal{P}(\Omega)$ for the map (3.7) with $\tilde{A}_j^{N,M} \tilde{\mu}_{j+1} = \frac{1}{M} \sum_{\iota=1}^M \delta_{V_T^{N,\iota}} := \frac{1}{M} \sum_{\iota=1}^M \delta_{X_{j+1}^{\iota}}$, where $V_T^{N,\iota}$ is the Euler approximation of the solution of the SDE (2.14):

$$V_{\tau_{\iota+1}}^{N,\iota} = V_{\tau_{\iota}}^{N,\iota} + \tilde{\alpha}(\tau_{\iota}, V_{\tau_{\iota}}^{N,\iota}, \tilde{\mu}_{j+1}^B) \Delta\tau + \Delta W_{\tau_{\iota}}, \quad V_{\tau_0}^{N,\iota} = 0, \quad \iota \in \{1, 2, \dots, M\}.\quad (3.10)$$

and we set $T = 1$, and $\Delta\tau := T/N$. Note that in (3.10), $V_{\tau_{\iota}}^N$ is purely an auxiliary process; $\tilde{\mu}_{j+1}^B$ is used for approximation of $\tilde{\mu}_{j+1}$ where the former stands for the ensemble particle approximation of the latter.

Hence, based on the discussions above, we design Algorithm 2 for the entire nonlinear filtering process, which is named the ensemble Schrödinger Bridge filter. A few remarks and implementation notes are made for Algorithm 2:

1. The entire algorithm is based on the idea of Schrödinger generative model which we discussed in section 1 which is training free and derivative free. The most computationally expensive step is just the forward propagation of each particle from the particle cloud through (3.10) which is parallelizable, hence the entire algorithm can be implemented efficiently.
2. In the algorithm, in general we could start with B initial particles $\mathbb{P}(X_0 | \mathcal{Y}_0)$ and proceed by generating M particles for the posterior step. In the current algorithm design, we take $M = B$. In fact, once the data assimilation passes burn-in time, one could produce arbitrarily large particle cloud for the posterior distribution, i.e. $M > B$.
3. The algorithm does not present any structure error as in [1] where in the update step, such error is introduced in the approximation for the score function of the posterior. In Algorithm 2 though, the mapping at the analysis step is approximated via: $\tilde{A}_j \tilde{\mu}_{j+1} \approx \tilde{A}_j^{N,B} \tilde{\mu}_{j+1} = \frac{1}{B} \sum_{\iota=1}^B \delta_{V_T^{N,\iota}}$ where errors are introduced only in the Euler-Maurayama discretization of the SDE (2.14) and the ensemble average approximation of the expectation in the drift term (3.8).
4. Importantly, (3.9) could suffer numerical overflow in implementation due to the large positive/negative arguments especially when the underlying dimension gets high. To mitigate the issue, one can rescale the terms in the exponential function in both the numerator and denominator according to the structure of the drift without introducing any bias. Direct implementation without proper scaling may also result in very noisy state estimates.

Algorithm 2 Algorithm for the ensemble Schrödinger Bridge filter (EnSBF)

Require: Initializing the following terms

- The model: f, g as in (3.1) and (3.2). The initial density $\mu_0 := \mathbb{P}(X_0|Y_0) := \frac{1}{B} \sum_{i=1}^B \delta_{X_0^i}$ which is a particle ensemble.
- Total number of filtering steps J . The time horizon $T = 1$, total number of temporal discretization N in the Euler scheme for the Schrödinger Bridge data generator. $\Delta\tau := \frac{T}{N}$.

1: **for** $j = 0, 1, 2, \dots, J - 1$ **do**

2: • Obtain $\mathbb{P}(X_{j+1}|\mathcal{Y}_j) = \frac{1}{B} \sum_{i=1}^B \delta_{\tilde{X}_{j+1}^i}$ based on $\mathbb{P}(X_j|\mathcal{Y}_j) = \frac{1}{B} \sum_{i=1}^B \delta_{X_j^i}$ using equation (3.1).

- Update $\mathbb{P}(X_{j+1}|\mathcal{Y}_j)$ to $\mathbb{P}(X_{j+1}|\mathcal{Y}_{j+1})$ by generating the particle ensembles $\frac{1}{B} \sum_{i=1}^B \delta_{X_{j+1}^i}$ via the Schrödinger Bridge map $\tilde{A}_j^{N,B} : \mathcal{P}(\Omega) \rightarrow \mathcal{P}(\Omega)$:

$$\tilde{A}_j^{N,B} \mathbb{P}(X_{j+1}|\mathcal{Y}_j) \approx \mathbb{P}(X_{j+1}|\mathcal{Y}_{j+1}) \quad (3.11)$$

which is realized by collecting the terminal state $V_T^{N,\iota}$ of the solution of the following discrete SDE: for $\iota = 0, \dots, N - 1$

$$V_{\tau_{\iota+1}}^{N,\iota} = V_{\tau_\iota}^{N,\iota} + \tilde{\alpha}(\tau_\iota, V_{\tau_\iota}^\iota, \frac{1}{B} \sum_{i=1}^B \delta_{\tilde{X}_{j+1}^i}) \Delta\tau + \Delta W_{\tau_\iota}^\iota, \quad V_{\tau_0}^{N,\iota} = 0, \quad \iota \in \{1, 2, \dots, B\}. \quad (3.12)$$

where the function $\tilde{\alpha}$ is defined in (3.9). Then $\tilde{A}_j^{N,B} \mathbb{P}(X_{j+1}|\mathcal{Y}_j) = \frac{1}{B} \sum_{\iota=1}^B V_T^{N,\iota}$.

3: **end for**

5. In the scheme above, all the particles started from location 0 in the SDE at the analysis step. In fact, it can be shown that one could construct $\mathbb{P} \in \mathcal{P}(\Omega)$ induced by a stochastic process such that it interpolates $\delta_a, a \in \mathbb{R}^d$ and the target distribution μ (see also [26]). The drift term then takes the following form:

$$\tilde{\alpha}(t, x, \tilde{\mu}) := \frac{\mathbb{E}_{Z \sim \tilde{\mu}}[(Z - x) \exp(-\frac{1}{2(T-t)}|Z - x|^2 + \frac{1}{2T}|Z - a|^2) \tilde{g}(Z)]}{(T - t) \mathbb{E}_{Z \sim \tilde{\mu}}[\exp(-\frac{1}{2(T-t)}|Z - x|^2 + \frac{1}{2T}|Z - a|^2) \tilde{g}(Z)]} \quad (3.13)$$

Implementation-wise, the benefit of this form is that one can select the starting position of initial ensemble particles more freely than just setting it to be 0. Such setup will be useful when the samples from distribution $\tilde{\mu}$ are far from zero in which case one can choose a to be the mean of the data from $\tilde{\mu}$.

6. Moreover, we note that the quality of the numerical approximation (3.9) for equation (3.8) relies on the qualities of the samples coming from $\tilde{\mu}_j$, and the function \tilde{g}_j which typically takes the form:

$$\tilde{g}_j \sim \exp\left(-\frac{1}{2}(g(X_{j+1}) - Y_{j+1})^T \Sigma^{-1}(g(X_{j+1}) - Y_{j+1})\right) \quad (3.14)$$

where Y_{j+1} are the state of the observational process. If data samples from $\tilde{\mu}_{j+1}$ are too far away from the mode of function \tilde{g}_j , the exponential decay behavior of (3.14) will render the Monte Carlo integration in (3.8) inefficient. As such, one could resort to other simulation techniques which could potentially improve the accuracy of approximation for the drift term. As a starter, inspired from the importance sampling technique, one can perform a change of measure for potential performance improvement.

To proceed, instead of using the $\{\tilde{X}_j^i\}_{i=1}^B$ particles from the prediction step, one can use an alternative proposal which takes into consideration the new observation Y_{j+1} :

$$\tilde{X}_j^i \sim \mathbb{Q}(X_{j+1}|X_j^i, Y_{j+1}). \quad (3.15)$$

That is, at the j th filtering step, one has available the ensemble particles $\{X_j^i\}_{i=1}^B$ and also the observation Y_{j+1} . Thus, samples are drawn from a proposal distribution $\mathbb{Q}(X_{j+1}|X_j^i, Y_{j+1})$ which uses all these information. Denoting $h_a(z, x) := \exp(-\frac{1}{2(T-t)}|z - x|^2 + \frac{1}{2T}|z - a|^2)$, and noting that $\tilde{\mu}_{j+1} = \mathbb{P}(X_{j+1}|Y_j)$ then after change of measure, the expectation can be replaced with

$$\mathbb{E}_{Z \sim \tilde{\mu}_{j+1}} [h_a(Z, x) \tilde{g}_j(Z)] \Rightarrow \mathbb{E}_{Z \sim \mathbb{Q}(x|X_j, Y_{j+1})} [h_a(Z, x) \frac{\mathbb{P}(Y_{j+1}|Z)\mathbb{P}(Z|X_j)}{\mathbb{Q}(Z|X_j, Y_{j+1})}]. \quad (3.16)$$

We noted that in (3.16), the choice of $\mathbb{Q}(x|X_j, Y_{j+1}) := \mathbb{P}(X_{j+1}|X_j)$ will recover the original algorithm. Thus defining $w_j^l := \frac{\mathbb{P}(Y_{j+1}|\tilde{X}_{j+1}^l)\mathbb{P}(\tilde{X}_{j+1}^l|X_j^l)}{\mathbb{Q}(\tilde{X}_{j+1}^l|X_j^l, Y_{j+1})}$ the new function α at each filtering stage can be expressed in the following form:

$$\bar{\alpha}_j(t, x) := \frac{\sum_{l=1}^B (\tilde{X}_{j+1}^l - x) h_a(\tilde{X}_{j+1}^l, x) w_j^l}{(T-t) \sum_{l=1}^B h_a(\tilde{X}_{j+1}^l, x) w_j^l} \quad (3.17)$$

As we will soon demonstrate in Section 3.2, the EnSBF demonstrates competitive performance over other nonlinear filters in mildly high dimensions. On the other hand, in Section 2.3, we have shown that the reverse SDE rising from the score-based diffusion model can be treated as a special case of the controlled SDE related to the Schrödinger bridge problem, which means that the EnSF filter can be linked to EnSBF. The figure below summarizes the idea of the design process and their connection.

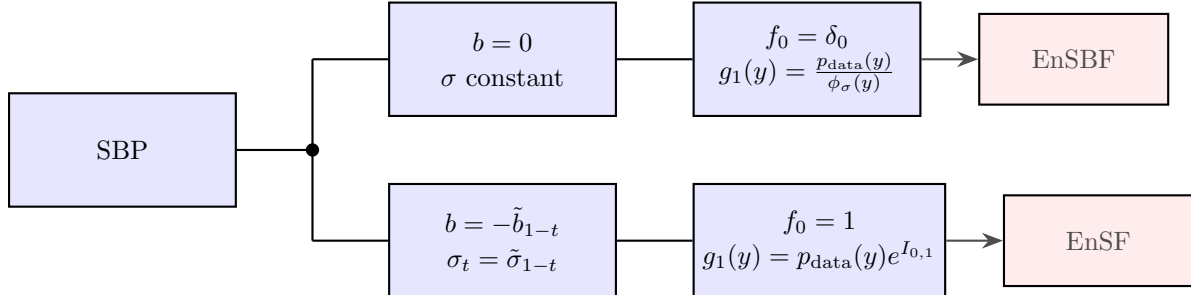


Figure 2: Flow chart of scheme design: starting from the SBP, the split node separates into the top part and down part. The first two vertical boxes corresponds to the reference SDE used to formulate the SBP; the next two blue vertical boxes corresponds to the solution strategies, i.e. the choices of f_0, g_1 . The dichotomy result in the EnSBF and EnSF filters accordingly.

More specifically, EnSBF and the EnSF algorithms are both originated from the SBP but via different constructions and the reference SDEs are different: the EnSBF is based on choosing $b_t = 0, \sigma_t = \sigma$ while EnSF relies on $b_t = -\tilde{b}_{1-t}$ and $\sigma_t = \tilde{\sigma}_{1-t}$ where $\tilde{b}_t, \tilde{\sigma}_t$ are defined in (2.64) and (2.65) as in Example 2.2. This leads to the different reverse/generating SDE processes and different simulation schemes. Though presenting model/structural error, the EnSF directly leverages sample approximation of the score function of X_{1-t} (solution to (2.66)) in (2.68) and it shows superb performance in high dimensions. This is because the gradient of a log function typically linearize a density kernel when it's (near) Gaussian which is one attractive feature of score functions. On the other hand, the EnSBF shows stronger performance in lower dimensions and it does not present structural error. As such, these two approaches complements each other and we propose to switch between these two on problems in different dimension regimes (with threshold being around 40) due to their connections. And we will leave the study of the integration of EnSF and EnSBF for accuracy improvement for future work.

3.2 Numerical examples for EnSBF

This section, we provide numerical examples for the designed algorithms.

1. Example 1 is a one-dimension example which demonstrates that EnSBF shows similar performance as the Ensemble Kalman filter and the Particle filter in low dimensions when only mild nonlinearity is given. The convergence behavior is also studied when the number of the temporal discretization and the ensemble sizes are increased respectively in posterior sample generation.
2. Example 2 is a 1-D double potential well problem which shows that the EnSBF presents better performance than both benchmarks given shocks in the signal.
3. Example 3 is a more in-depth comparison between PF and EnSBF: a one-step filtering procedure is designed where the prior, the likelihood and the posterior densities are all known analytically. The study shows that even when a large ensemble size is taken, the EnSBF still outperforms the PF in terms of Posterior approximation.
4. Example 4 is the Lorenz 96 model where the performance of EnSBF is tested under various dimensions (4 to 100), given the signal goes through linear observation. The performance is compared against EnKF, PF and EnSF. The test result shows that EnSBF performs reasonably well in lower dimensions while the predictions tend to deteriorate by showing larger fluctuation around the true signals. The EnKF shows overall good performance due to the relatively mild nonlinearity in the underlying dynamics. PF shows strong performance in a low dimension regime but fails in higher dimensions (≥ 20). EnSF shows weak performance in a low dimension environment under relatively large observation noise, but it demonstrates superior behavior when the dimension gets high (≥ 40).

Finally, when the signal goes through nonlinear transformation in the observation process, the performance of EnSBF is observed to deteriorate quickly once it goes above 40.

3.2.1 Example 1: the sine function.

In this example, we consider the following simple 1-D dynamics:

$$X_{j+1} = \alpha \sin(X_j) + \sigma \xi, \quad \xi \sim \mathcal{N}(0, 1) \quad (3.18)$$

$$Y_{j+1} = X_{j+1} + \gamma w, \quad w \sim \mathcal{N}(0, 1) \quad (3.19)$$

In this example, we set $\alpha = 2.5$, $\sigma = 0.2$ and $\gamma = 1.0$. We compare the performance of the three nonlinear filters, namely the Ensemble Kalman filter (EnKF), the particle filter (PF) and the Ensemble Schrödinger Bridge filter under this parameter setup. For the experiments, we choose the particle ensemble size to be 500 and the number of temporal discretization to be 100 for the SDE in EnSBF at each analysis step. It is noted in figure 3-a that all three filters show decay trend in terms of the smoothed RMSE. As expected, the EnKF slightly underperforms compared to PF and EnSBF due to the nonlinearity in the dynamics (3.18). In the meantime, since this is an one dimensional example and the ensemble size is chosen to be large, the PF and the EnSBF demonstrate similar performance.

To study the convergence behavior of the EnSBF for 800 filtering steps, we first fix the ensemble size to be 200 and change the number of Euler discretization N . We run the tests for 50 times and computed the average smoothed RMSE for presentation. It is observed from 3-b that the smoothed RMSE decays as the number of discretization number N increases in (3.10). This is as expected as the quality of the generated particles rely on the accuracy of the approximated solution of the diffusion SDE (2.14).

We then fix the number of temporal discretization N and change the ensemble size of the particles B . We run the tests for 50 times and computed the average smoothed RMSE for presentation. It is observed from 3-c that the smoothed RMSE also demonstrates decay behavior which is as expected: the approximation of the drift term relies on the number of the particles used for computations of expectation in (3.9).

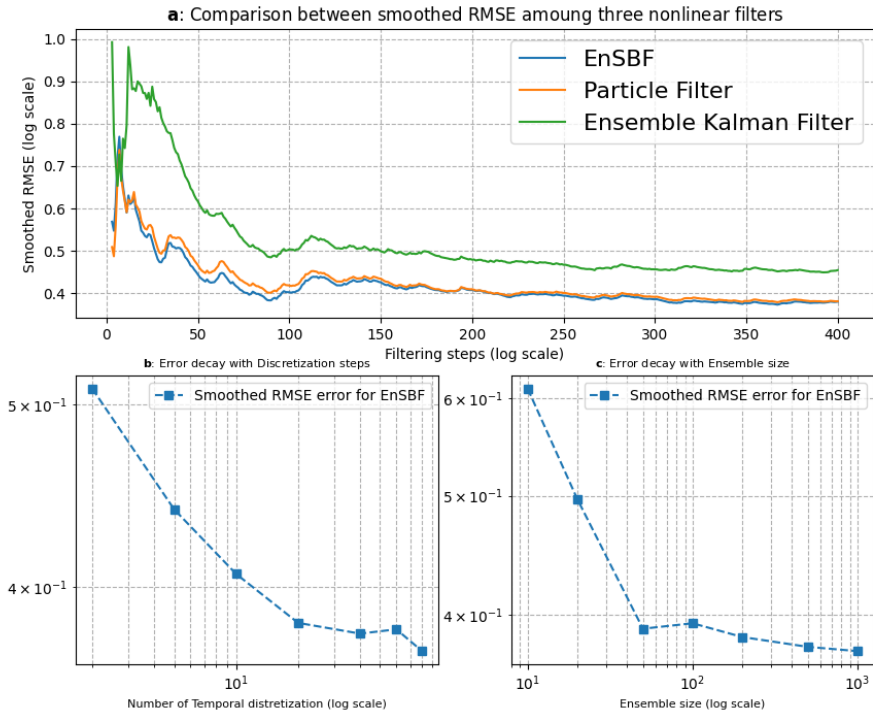


Figure 3: a: comparison between the smoothed RMSE among the three nonlinear filters. b: Error decay with respect to the number of temporal discretization N in the diffusion SDE, holding the ensemble size B fixed. c: Error decay with respect to the size of the particle ensemble, holding N fixed

3.2.2 Example 2. The 1-D potential well

The second example is the double potential well where the drift term is given by the function $-4x(x^2 - 1)$. The given dynamics is as follows:

$$S_{n+1} = S_n - (4.0 \cdot S_n(S_n^2 - 1))\Delta t + \beta\sqrt{\Delta t}\omega_n \quad (3.20)$$

$$M_{n+1} = S_{n+1} + \gamma_{n+1} \quad (3.21)$$

The particles propagate according to (3.20), and the observation process is based on process (3.21). At every 40 steps, the states are manually switched between 1 to -1 . Note that it is easy for the nonlinear filter to track the stationary state while hard to effectively respond to the sudden state change.

In this one dimensional example we focus on the comparison between filtered results from various nonlinear filters, namely the Ensemble Kalman Filter (EnKF), the particle filter (PF), the ensemble Schrödinger Bridge filter (EnSBF) and its variants: the EnSBF with measure change (EnSBF_I). We set $\gamma \sim \mathcal{N}(0, 0.1)$ for all time steps and $dt = 0.1$. We comment on the tests results presented in Figure 4 with the exact states shown in blue, the EnSBF shown in yellow, EnSBF_I in green, PF is in red and ensemble KF in purple.

- i.) In the case (4a) where a large ensemble size is taken (1000) and the noise level is set to be $\beta = 0.3$ in (3.20), all nonlinear filters are performing but with EnSB filter showing more accurate state tracking ability.
- ii.) In the case (4b) where the same number of particle is taken (1000) but with noise level tuned down ($\beta = 0.2$), neither the EnKF or PF are performing now. This phenomenon is due to the fact that the particle filters heavily rely on the quality of the ensemble particles for distribution approximation. When

there is a sudden state change, the state model retains a force that attracts the model to the bottom. Thus, the information of the particle concentrates heavily at the bottom of the potential which will lead to smaller variance of the cohort. This in turn will result in sparse particles at the tail of the distribution. The EnKF fails due to the highly nonlinear nature of the example while EnKF relies heavily on the Gaussian assumption, and it may not be sufficient to capture the non-Gaussian nature in the posterior. However, both EnSBF approaches are still performing.

- iii.) In the case (4c) where the ensemble size is reduced to 20 with the noise level kept at $\beta = 0.3$, the two SB filters and the EnKF still perform with the SB filter demonstrating slightly better performance. It is well known that EnKF relies on the Gaussian assumption, hence a reduction on the ensemble size will not significantly impact the performance in this case. In contrast, PF stores the density information solely in the ensemble particles, so when the ensemble size is small, PF fails to produce an accurate posterior. Overall, this shows that the designed method does not require a large number of particles to capture the statistical feature of the distribution in between filtering steps, a large improvement than the particle filter which usually needs a large particle size for the algorithm to converge (compare to 4a).
- iv.) Lastly in (4d), We use an ensemble size of 20 and reduce the noise in the signal to $\beta = 0.1$. In this case, the performance of the original EnSBF start to deteriorate. Both the EnKF and PF fail to perform while the EnSF still demonstrates some tracking ability.

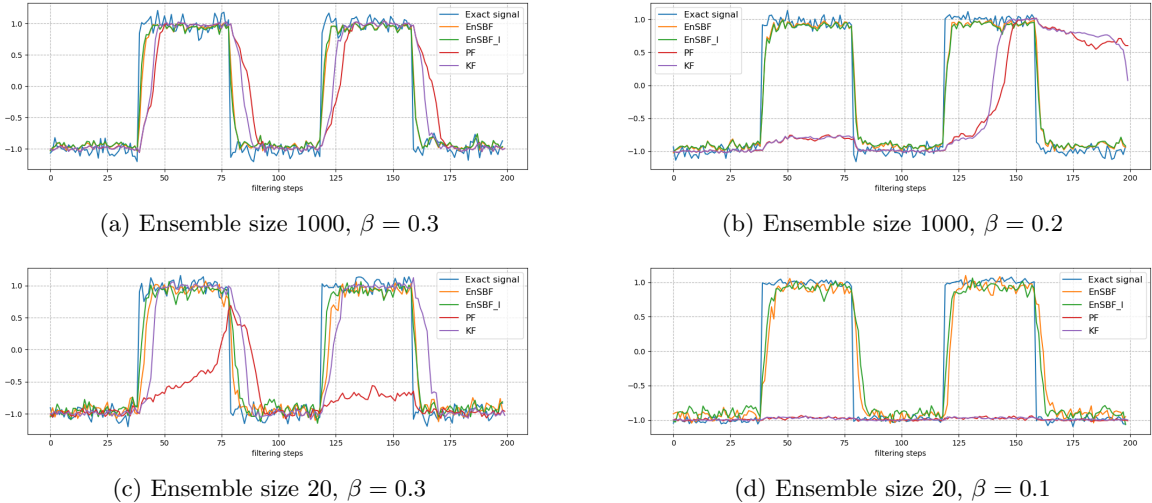


Figure 4: Comparison of state tracking among nonlinear filters

3.2.3 Example 3, Further comparison between EnSBF and PF

For a third example, we design a filtering step (one-step) where both the prior, the likelihood are assumed to be available in an analytic form such that the posterior can also be analytically calculated. More specifically, let the prior/likelihood be given as Gaussian mixture/Gaussian:

$$\mathbb{P}(X_{j+1}|\mathcal{Y}_j) = \frac{1}{8\pi\sigma^2} \sum_{k=1}^4 \exp\left(-\frac{|x - \mu_k|^2}{2\sigma^2}\right) \quad \text{Prior density} \quad (3.22)$$

$$\mathbb{P}(Y_{j+1}|X_j) = \frac{1}{2\pi\epsilon^2} \exp\left(-\frac{|x - \mu_0|^2}{2\epsilon^2}\right) \quad \text{Likelihood density} \quad (3.23)$$

$$\mathbb{P}(X_{j+1}|\mathcal{Y}_{j+1}) = \frac{1}{4} \sum_{k=1}^4 \frac{1}{2(\sigma^2 + \epsilon^2)} \exp\left(-\frac{|\mu_k - \mu_0|}{2(\sigma^2 + \epsilon^2)}\right) \mathcal{N}(x|m_k, \Sigma_k) \quad \text{Posterior density} \quad (3.24)$$

where $m_k = \frac{\epsilon^2 \mu_k + \sigma^2 \mu_0}{\sigma^2 + \epsilon^2}$, $\Sigma_k = \frac{\sigma^2 \epsilon^2}{\sigma^2 + \epsilon^2} I$. For this example, we choose $\mu_0 = (1.2, 0.0)$, $\mu_1 = (1.5, 1.0)$, $\mu_2 = (1.0, -1.0)$, $\mu_3 = (-1.5, 1.0)$, $\mu_4 = (-1.0, -1.0)$, $\sigma = 0.2$ and $\epsilon = 0.25$. To implement the test, let the samples

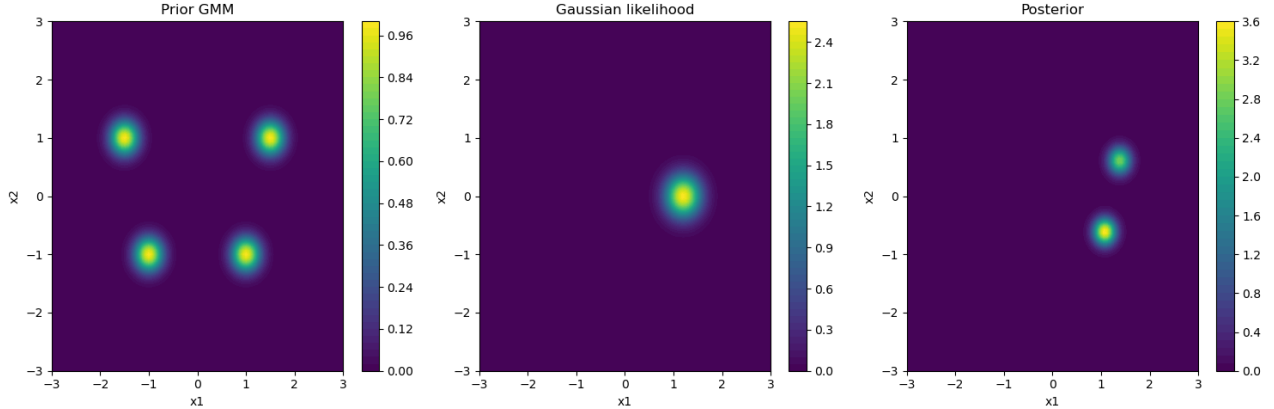


Figure 5: Prior, likelihood and posterior density plots for the Gaussian Mixture models. The true posterior presents multi-modal behavior.

from prior be given via an ensemble of particles. Then, to perform data assimilation, we implement the task by using both the PF method and EnSBF method. For comparison purposes we use ensemble size of 2500 particles. The results are presented in 6. In Figure 6, the left figure shows the heatmap of the analytical posterior density

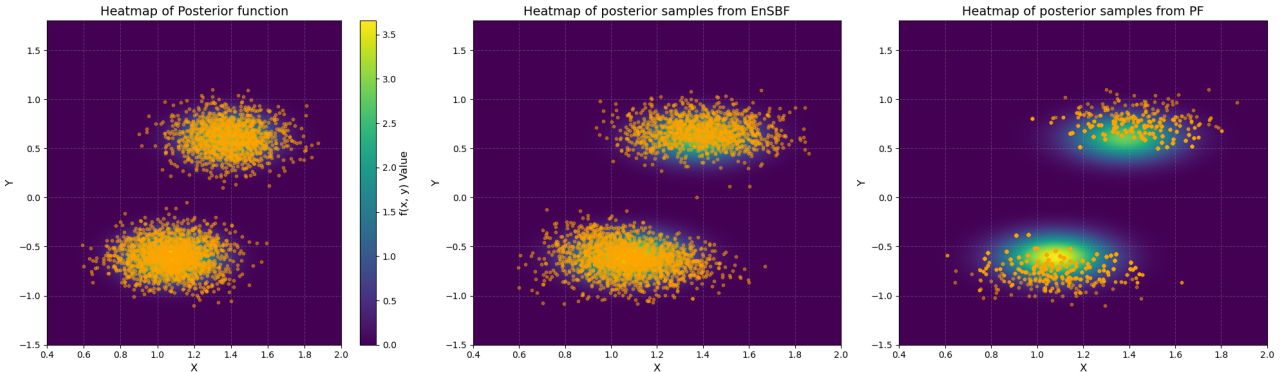


Figure 6: Posterior density approximation result by using the EnSBF and PF approaches. The left figure shows the exact posterior densities and the ensemble particles via exact simulation. The mid/right figures are the particle ensembles obtained via EnSBF and PF methods. The EnSBF demonstrates superiority over PF regarding density approximation in this case.

and the corresponding samples from the same. The mid figure shows the posterior ensemble obtained via the EnSBF method while the right figure is obtained via the PF method. It is noted that compared to the EnSBF, PF does not capture the posterior density well and that the resampling step produces ensemble with many repeated particle locations. This shows that EnSBF does a better job than PF in data assimilation when the posterior density is multi-modal.

3.2.4 Example 4, the 96 Lorenz model

For the last example, we consider the Lorenz-96 model. *The goal is to study EnSBF's performance under different dimensions.* The performance of the following four nonlinear filters are compared: PF, EnSBF, EnSF and EnKF. The overall observations are summarized as follows:

- The EnSBF overall performs well especially in low dimension regime (comparable to PF). However, its performance deteriorates when the dimension gets high and the predictions start to become noisy which tend to fluctuate around the true signal.
- For the Lorenz 96 model, EnKF still performs well because there is no sudden state change like the double potential well example. The algorithm design in EnKF can overall capture the example's underlying nonlinear structure.
- The EnSF does not perform well in low dimension regime especially when the noise in the observational process is high. This is mainly due to the existence in of model/structural error in the algorithm design. The EnSBF overcomes such limitation and demonstrates much more competitive performance. On the other hand, when the underlying dimension becomes high, EnSF beats other filters including EnKF which is as observed in [6].

We consider the dynamics in the following form

$$dx_t^i = \left((x_t^{i+1} - x_t^{i-2})x_t^{i-1} + F \right) dt + \sigma^i dW_t^i, \quad i = 1, 2, \dots, d, d \geq 4 \quad (3.25)$$

$$Y_t = \alpha X_t + \gamma_t, \quad \gamma_t \sim \mathcal{N}(0, \Gamma) \quad (3.26)$$

In this example, we note that the high nonlinearity in the dynamics (3.25) make the dynamics difficult to track when the dimension d gets high.

Experimental results show that (figure-7) in the low dimension regime $d = 4$ with forcing $F = 8$, all filters perform well given sufficiently large ensemble size $B = 600$ with $\Gamma = 0.04I$ except for the EnSF. This is because there is model/structural error present in EnSF: the score function of the posterior is constructed via a simple linear combination between the score function of the estimated prior and that of the likelihood. Such bias is not present in the EnSBF approach or particle filter.

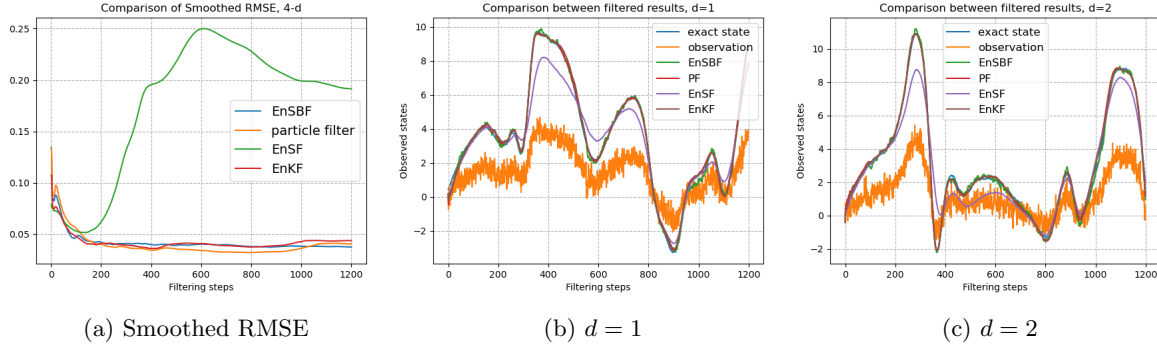


Figure 7: Comparison of state tracking among nonlinear filters, Lorenz 96. Ensemble size 600, $\alpha = 0.2$

In the case when the dimension is increased to $d = 8$, under the smaller observational noise $\Gamma = 0.15^2 I$, we increase the ensemble size to 800 so that the particle filter will perform(figure 8). It is observed that the EnKF shows better predicting power by showing slightly lower RMSE (per dimension). EnSBF demonstrates similar accuracy to PF while EnSF has issue in tracking the peak and troughs of true signals due to presence of structural error. See Figure (8b-8c).

Keeping all other parameters the same, we further test the algorithm performance at a higher dimension of $d = 20$. In this case, the PF fails to perform which shows constantly increasing RMSE. This is due to the curse of dimensionality: more particles are needed to store the information of the filtering distribution to track the state. For this reason we do not present its RMSE. Since $d = 20$ still corresponds to a relatively low dimension, both EnSBF and EnKF show better performance. See Figures 9b - 9c for more details.

For a higher dimensional example, we increase the dimension to $d = 100$, increase the forcing term to $F = 10$ and change $\Gamma = 0.1^2 I_d$. It is now observed that EnSF demonstrates its strength in a higher dimension setting

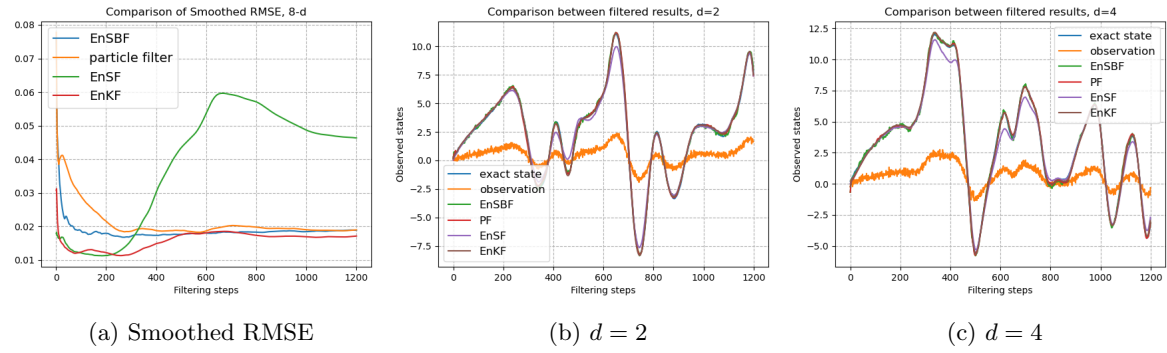


Figure 8: Comparison of state tracking among nonlinear filters, Lorentz 96. Total dimension= 8. Ensemble size 800. $\alpha = 0.2$

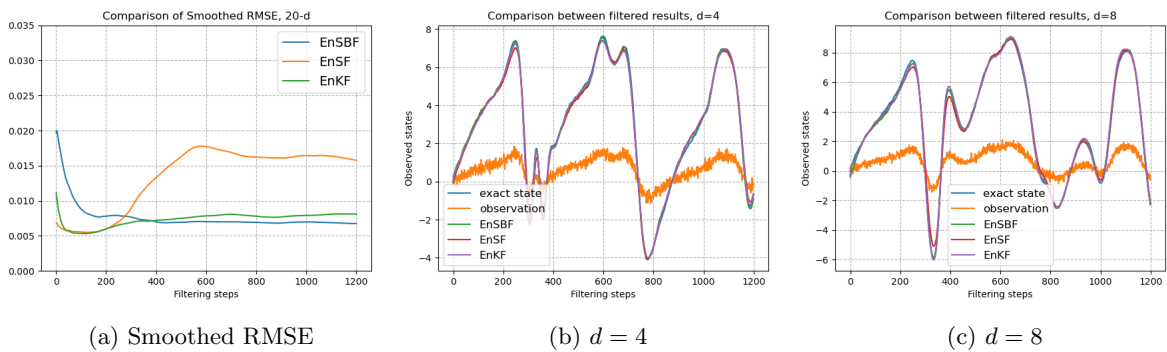


Figure 9: Comparison of state tracking among nonlinear filters, Lorentz 96. Total dimension= 40, Ensemble size = 800, $\alpha = 0.2$

by showing an overall smaller RMSE. The EnSBF performance is overall worse than EnSF (green curve in 10b-10c): the estimates now fluctuates slightly around the signal. See Figures 10b - 10c for more details.

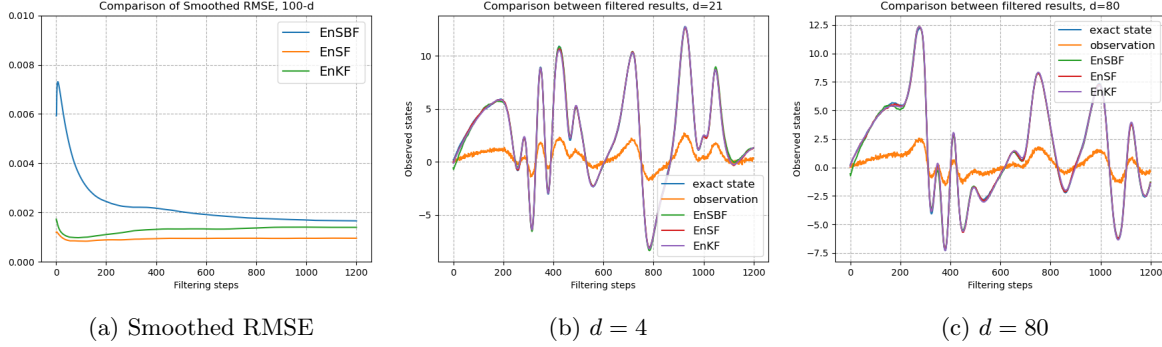


Figure 10: Comparison of state tracking among nonlinear filters, Lorentz 96. Total dimension= 100, Ensemble size = 500, $\alpha = 0.2$.

Nonlinear observation

To test the case where the observation is also nonlinear, we change (3.26) to the following:

$$Y_t = \arctan(X_t) + \gamma_t, \quad \gamma_t \sim \mathcal{N}(0, \Gamma), \quad \Gamma = 0.1^2 I_d \quad (3.27)$$

In this case, in the low dimension regime, the observation is consistent with the case where the observation process is linear. In higher dimension $d = 40$, using ensemble size of 100 and signal process set up same as before, we obtain results in figure 11. It is noted that EnSBF shows overall competitive performance compared to the state of the art EnSF and EnKF. However, in our further experiments, it is observed that the performance of the EnSBF deteriorates significantly once the dimension gets higher than say $d = 50$ dimensions.

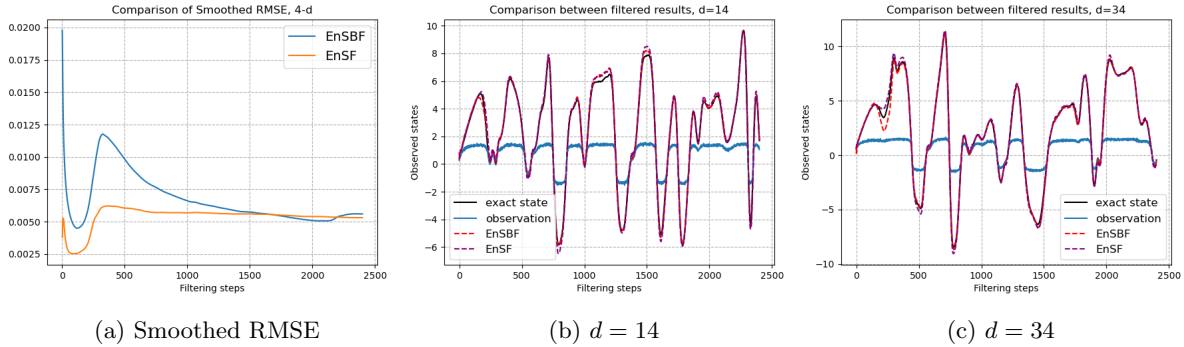


Figure 11: Comparison of state tracking among nonlinear filters, Lorentz 96. Total dimension= 40, Ensemble size = 500.

4 Conclusion and future work

In this work, we developed a novel nonlinear stochastic filter, namely the ensemble Schrödinger Bridge filter which demonstrates overall competitive performance over the classical ensemble Kalman filter and the Particle filter (PF) in a mildly high dimensional environment given nonlinear dynamics under chaotic setup. Such method is also found to rely less on the ensemble size of the particles than the particle filter. This approach

is both training free and derivative free. The algorithm design also demonstrates no model error which is a limitation for the EnSF [1]. In lower dimension regime, it demonstrates more reliable performance than the EnSF. Currently, the limitation of this approach is that it is not performing stably in very high dimensions. This deficiency though is not due to the Schrödinger Bridge data generator itself but the design of the analysis step based on the SDE related to SBP. Hence, the future work will focus on refining the algorithm so that it will also perform in very high dimensions. We will also work to establish a convergence proof for the EnSBF.

References

- [1] F. Bao, Z. Zhang, and G. Zhang, *A Score-based Filter for Nonlinear Data Assimilation*, Journal of Computational Physics, 514, 113207, 2024.
- [2] F. Bao, Y. Cao, and P. Maksymovych, *Backward sde filter for jump diffusion processes and its applications in material sciences*, Communications in Computational Physics, 27 (2020), pp. 589–618
- [3] F. Bao, N. Cogan, A. Dobreva, and R. Paus, *Data assimilation of synthetic data as a novel strategy for predicting disease progression in alopecia areata*, Mathematical Medicine and Biology: A Journal of the IMA, (2021)
- [4] S. Liang, H.Tran, F. Bao, H. G. Chipilski, P.J.V. Leeuwen, G. Zhang. *Ensemble score filter with image inpainting for data assimilation in tracking surface quasi-geostrophic dynamics with partial observations*. <https://arxiv.org/pdf/2501.12419.pdf>.
- [5] H.G. Chipilski, F. Bao, S. Liang, G. Zhang, J.S.Whitaker *Nonlinear Ensemble Filtering with Diffusion Models: Application to the Surface Quasi-Geostrophic Dynamics*, 105th AMS Annual Meeting, 2025.
- [6] F.Bao, Z.Zhang, G.Zhang. *An ensemble score filter for tracking high-dimensional nonlinear dynamical systems*. Computer Methods in Applied Mechanics and Engineering. Volume 432, Part B, 1 December 2024, 117447.
- [7] G. Evensen, *The ensemble Kalman filter for combined state and parameter estimation: Monte Carlo techniques for data assimilation in large systems*, IEEE Control Syst. Mag., 29 (2009), pp. 83–104.
- [8] B. Ramaprasad, *Stochastic filtering with applications in finance*, 2010.
- [9] M. Hamdouche, P.Henry-Labordere, and H. Pham. (2023). *Generative modeling for time series via schrödinger bridge*. arXiv:2304.05093.
- [10] Yang Song, Sahaj Garg*, Jiaxin Shi, and Stefano Ermon Sliced Score Matching: A Scalable Approach to Density and Score Estimation. *In the 35th Conference on Uncertainty in Artificial Intelligence*, 2019
- [11] Yang Song. *Generative Modeling by Estimating Gradients of the Data Distribution*. Blog Post, <https://yang-song.net/blog/2021/score/>.
- [12] Y. Song, S. Ermon. Generative Modeling by Estimating Gradients of the Data Distribution *Advances in Neural Information Processing Systems*, pp. 11895–11907. 2019.
- [13] Yang Song, Jascha Sohl-Dickstein, Diederik P. Kingma, Abhishek Kumar, Stefano Ermon, and Ben Poole. Score-based generative modeling through stochastic differential equations. *International Conference on Learning Representations (ICLR)*, 2021. <https://openreview.net/forum?id=PxTIG12RRHS>.
- [14] Jascha Sohl-Dickstein, Eric Weiss, Niru Maheswaranathan, and Surya Ganguli. Deep unsupervised learning using nonequilibrium thermodynamics. *In International Conference on Machine Learning*, pages 2256–2265, 2015

[15] Jonathan Ho, Ajay Jain, and Pieter Abbeel. Denoising diffusion probabilistic models. In *Advances in Neural Information Processing Systems (NeurIPS)*, 2020. <https://arxiv.org/abs/2006.11239>.

[16] Pascal Vincent. A connection between score matching and denoising autoencoders. *Neural Computation*, 23(7):1661–1674, 2011. https://www.iro.umontreal.ca/~vincentp/Publications/smdae_techreport.pdf

[17] E. Bernton, J. Heng, A. Doucet, and P. E.Jacob, (2019). *Schrödinger bridge samplers*. <https://arxiv.org/abs/1912.13170>

[18] V. D. Bortoli, J. Thornton, J.Heng, A. Doucet (2023). *Diffusion Schrödinger bridge with applications to score-based generative modeling*.<https://arxiv.org/abs/2106.01357>

[19] T. Chen, G.-H. Liu, and E. A. Theodorou, (2023a). *Likelihood training of Schrödinger bridge using forward-backward sdes theory*. <https://arxiv.org/abs/2110.11291>.

[20] Y. Shi, V. D. Bortoli, A. Campbell, and A. Doucet (2023). *Diffusion Schrödinger bridge matching*. <https://arxiv.org/abs/2303.16852>.

[21] Z. Chen, G.He, K. Zheng, X.Tan, and J.Zhu (2023c). *Schrödinger bridges beat diffusion models on text-to-speech synthesis*. <https://arxiv.org/abs/2312.03491>.

[22] G.H.Liu, A.Vahdat, D.A. Huang, E. Theodorou, W. Nie, and A. Anandkumar (2023). *I2sb:Image-to-image schrodinger bridge*. In International Conference on Machine Learning (ICML).

[23] Stromme, A. (2023). *Sampling from a Schrödinger bridge*. Proceedings of The 26th International Conference on Artificial Intelligence and Statistics, volume 206 of Proceedings of Machine Learning Research, pages 4058–4067. PMLR.

[24] P. Dai Pra, *A stochastic control approach to reciprocal diffusion processes*. (1991). *Applied Mathematics and Optimization*, 23(1):313–329.

[25] G. Wang, Y.Jiao, Q.Xu, Y. Wang, C.Yang. *Deep Generative Learning via Schrödinger Bridge*, PMLR 139, 2021.<https://proceedings.mlr.press/v139/wang21l/wang21l.pdf>.

[26] Hanwen Huang. *One-step data-driven generative model via Schrödinger Bridge*. <https://arxiv.org/abs/2405.12453>.

[27] Y. Chen, T. T. Georgiou, and M. Pavon (2021). *Optimal transport in systems and control*. Annual Review of Control, Robotics, and Autonomous Systems, 4(Volume 4, 2021):89–113.

[28] I.Goodfellow; J. Pouget-Abadie; M. Mirza;B. Xu; D. Warde-Farley; S. Ozair; A. Courville; Y. Bengio (2014). *Generative Adversarial Nets*. Proceedings of the International Conference on Neural Information Processing Systems (NIPS 2014). pp. 2672–2680.

[29] M. Arjovsky, S.Chintala, L.Bottou, *Wasserstein Generative Adversarial Networks*. International Conference on Machine Learning. PMLR: 214–223

[30] Danilo Jimenez Rezende and Shakir Mohamed. Variational inference with normalizing flows.<https://arxiv.org/abs/1505.05770>

[31] Laurent Dinh, Jascha Sohl-Dickstein, Samy Bengio. *Density estimation using real NVP*. 2016. <https://arxiv.org/abs/1605.08803>

[32] K.Law, A.Stuart, K.Zygalakis. *Data Assimilation, A Mathematical Introduction* 2016. Texts in Applied Mathemtatics, Vol 62, ISSN 2196-9949, Springer International Publishing Switzerland 2015.

- [33] C. Léonard. *A survey of the Schrödinger bridge problem and some of its connections with optimal transport.* DYNAMICAL SYSTEMS, 34(4):1533–1574, 2014.
- [34] Y.Chen, T.T.Georgiou, and M.Pavon. *Stochastic control liasons: Richard sinkhorn meets Gaspard Monge on a Schrödinger bridge.* arXiv preprint arXiv:2005.10963, 2020.
- [35] J. Huang, Y. Jiao, L. Kang, X. Liao, J. Liu, Y. Liu *Schrödinger-Föllmer Sampler: Sampling without Ergodicity* <https://arxiv.org/abs/2106.10880>.
- [36] W. Tang, H. Zhao, *Contractive Diffusion Probabilistic Models* <https://arxiv.org/pdf/2401.13115.pdf>.